DESIGN RULES FOR A CFRP OUTER WING

Lars Herbeck and Holger Wilmes
DLR, Institute of Structural Mechanics, Lilienthalplatz 7,
38108 Braunschweig, Germany

Keywords: *CFRP, Design Rules, Outer Wing, Bolted Joint, Rib, Stability*

Abstract

Design rules for composite components are an effective method for design engineers to realize a design with an optimal weight. They help identify the decisive parameters and point out the physical correlations.
The process of setting up and verifying design rules for the components of a CFRP outer wing are explained in this report by taking bolted joints and stability for ribs and spars as an example.
Analytical calculation methods and a comparison with experiments in particular are addressed here.

1 Introduction

The development and design of new large aircraft like the Airbus A380 leads to increased dimensions and subsequently to higher load levels. Therefore, the use of advanced materials and design concepts is essential. CFRP is intended for large, highly-loaded structures such as the wing. Apart from the excellent specific values of CFRP in terms of stiffness and strength, composite materials offer additional design parameters like the stacking sequence which lead to an increase of flexibility in the structural design. In order to make use of these new options, the design engineer requires fast calculation methods for the dimensioning of CFRP components. Apart from the advantages of fast calculation analyses, design rules offer the possibility of detecting physical interdependencies, thus enabling the detection of the main parameters in the laminate design.

The Institute of Structural Mechanics of the German Aerospace Center (DLR) was commissioned by Airbus Germany to develop design rules for a CFRP outer wing. Working in joint teams, these design rules were set up and verified for spars, ribs, thick laminates and mechanical joints. A substantial part of this work was the development of test set-ups with realistic load and clamp conditions.

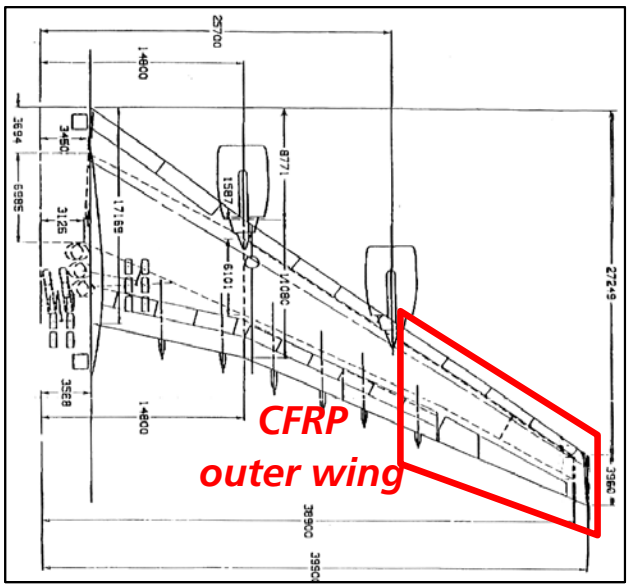

Fig. 1. Wing of a Megaliner: inner wing made of aluminum and outer wing made of CFRP

Analytical calculations were primarily made for the set-up of optimized design rules. The standard design methods in aerospace technology as provided by JAR and German aerospace design handbook (LTH) (Part: Handbook of Structural Calculation) were also taken into account. Standard finite element programs were used for detailed analyses as well. In order to prove the design rules, the above-mentioned tests were evaluated extensively and the design rules that were obtained are now part of the LTH.

The creation of design rules for a CFRP outer wing are shown in this report with two

examples. A design rule for the calculation of bolted joints is explained and the calculation, optimization, and testing by means of experiments are shown with the example of the stability of unstiffened, notched rips.

1.1 Bolted joints

The currently used Airbus design method for large CFRP structures, especially for highly-loaded areas, is based on bolted joints for structural assembly. Up to now, almost no experience is available on the required laminate thickness from 15 mm up to 30 mm as used in a CFRP outer wing. A total of 900 specimens (notched strips and bolted joints) were tested to obtain reliable data for the design and proof of these types of structures. The experiments included the examination of typical parameters. The aim was to determine the influence of different loading conditions on notches including the change of the load distribution in a joint and to figure out the effect of secondary bending on the materials' strength. The test program comprises examinations on single and double-shear joints, different rows of bolts, several laminate stacking sequences, various bolt geometries and materials for different laminate thickness from 5 mm up to 30 mm. These parameters are examined for static and fatigue loading due to tension and compression. The results were compared with detailed analytical and numerical analyses in order to set up design rules for joints in CFRP. This guideline provides a program for the design of joints. Furthermore, an option is now available to optimize the available parameters in reference to the strength of the joint.

1.1 Ribs

The design rules of ribs allow for the dimensioning of loaded areas where strength is the failure criterion. Different cut-outs with various geometries were taken into account and optimized. For loaded areas in terms of stability, the influence of shear, compression, and combined loadings were investigated. In this case the stacking sequence and additional stringer stiffening were analyzed by taking local and global buckling into consideration. These design rules were verified by 108 coupon and component tests.

2 Design Rules for Bolted Joints

A dimensioning guideline was created for the dimensioning of the bolted joints found in the CFRP outer wings of a megaliner in order to secure the design. A program with CFRP samples (carbon fiber reinforced polymers) was carried out. Different parameters of bolted joints that typically occur were recorded against the background of the great wall thickness of such a wing especially in the 15 mm to 30 mm interface of inner and outer wing.

2.1 Bolted Joints for Fiber Composite Materials

Bolted joints are widely used in the aircraft industry. The advantages of these joints are that they can be undone and that they ensure a reliable process with few risks. On the other hand, one inevitable disadvantage is a reduction in strength due to a concentration of stress in the notches which must be taken into consideration during the design process of the component.

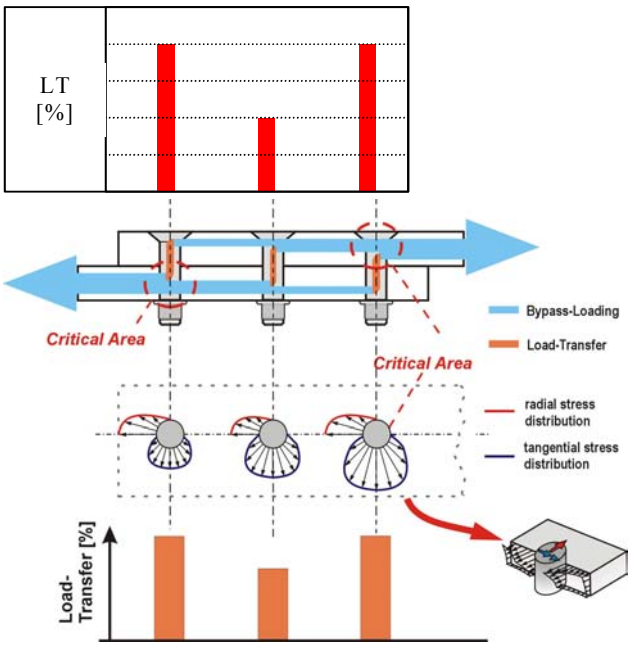

Fig. 2. Force progression of a single-shear, triple-rowed joint.

In order to design a bolted joint made of CFRP it is necessary to identify its critical area. The force progression is depicted with the example of a single-shear, triple-rowed, bolted joints (Fig. 2).

It becomes clear that highest loads occur in the area of the outer bolts which is comparable to the distribution of shear stress in bonded joints.

In addition to these irregular distributions of force, greatly varying loading of the joint piece occurs along the length of the connecting area. Loading of each subsequent notch increases with each bolt since the load that was previously transmitted is transferred past the hole as a bypass which results in increased stress (tangential tension). The notch on the first (or last) bolt of each joint piece is the most highly stressed area of the whole joint (Fig. 2) since the tangential tension here consisting of load transfer and bypass load is the most highly superimposed.

Due to the bypass loading, maximum stress occurs in the laminate at the edge of the hole in the area of the most narrow cross-section. The laminate in this area around the hole fails accordingly. Excess tension caused by bypass loading is primarily determined by the laminate set-up [1]. In addition, geometric measurements, the arrangement of the bolts (pitch, edge distance), and particularly the absolute hole size influence the strength since a so-called hole-size effect can be observed in fiber composites [2].

The load is transferred by the bearing between the bolt and the edge of the hole. This results in radial tension at the edge of the notch because of the bearing and tangential tension which, in turn, is due to load diversion of the transmitted force around the hole.

Several possibilities of laminate failure in bolted joints are the result.

Failure occurs in the rest of the cross-section (tension failure), as can also be observed in holes without loads, and at the pressure point of the bolt (bearing of the hole, shear out failure) as well. In addition, mixed forms occur in bolted joints during failure (clearage tension failure) (see also [3]).

Influencing parameters in bolted joints are geometric measurements such as width, edge distance, thickness and hole diameter, the laminate set-up, (number of plies in a certain direction), abatement, material, stacking sequence, and fitting of the joint. Parameters such as environmental influences, bolt material and clamping can influence the strength of such joints [4], [5].

2.2 Design Rule for Bolted Joints

In order to create a dimensioning guideline for multi-rowed bolted joints, it is assumed that the fractured body can be seen as linearly elastic in the whole area. For this reason, any inelastic procedures must be limited to small areas that correspondingly can be microscopically neglected. This approach particularly applies to failure in the form of a brittle fracture that can be observed in fiber composites particularly when fiber plies are positioned in the direction of the load.

Similar to the K concept of the linear fracture hypothesis, it is assumed that the linear elasticity theory in the area of maximum tension around the notch no longer represents a sufficient specification. The microscopic intermediate fiber fractures in the material run along the fiber orientation and bring with them concentrations of inner forces (see Fig. 3).

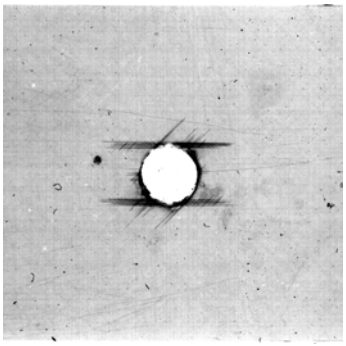

Fig. 3. Intermediate fiber fracture in the area of a notch (x-ray)

In order to formulate a fracture criterion, a description of the definition for tension is chosen. The influence of the high-energy area is taken into account by k_i (notch stress factor) which is a type of excess tension. The tension

can therefore be formulated in the area of the notch, σ_K, in the following context:

$$\sigma_K = k_i \cdot \sigma_B = k_i \cdot \frac{F}{A} \quad (1)$$

Factor k_i shows to what extent the applied (total) tension, σ_B, is elevated in the area of the notch and therefore which tension occurs in the notch (σ_K).

In order to formulate a fracture hypothesis, it is now assumed that the notched body fails when the tension of the notch corresponds with the strength of the (unnotched) laminate, $\sigma_{Lam.}$. The following is postulated for the fracture:

$$\sigma_{Lam.} = \sigma_K \quad (2)$$

A number of well-known concepts in scientific literature are based on similar principles [6].

It is assumed that the fractured body can be microscopically regarded linearly elastic. As a result, the following notch load levels can be superimposed:

$$\sigma_K = \sum_{i=1}^{N} k_i \cdot \sigma_B \quad (3)$$

The highest notch load level in bolted joints results from the shares that are transferred into the area of the first (last) bolt by means of bypass loading and load transfer:

$$F_{LT} = LO \cdot F_{ges}, \; F_{BY} = (1 - LO) \cdot F_{ges} \quad (4)$$

and therefore the following applies for the notch loading:

$$\kappa_k = (1 - LO) \cdot \kappa_{BY} + LO \cdot \kappa_{LT} \quad (5)$$

The load transfer takes place by contact stresses of the bore edges and bolt. Depending on the number of notches in the joint and the thickness of the joint piece, the bolt is additionally stressed by bending. Bending the bolt causes an uneven surface pressure over the wall thickness of the component and leads to a reduction in strength which must taken into account in the k_{LT} factor

Jarfall [7] has already presented a similar model for the calculation of cyclically loaded metal joints in which excess tension can be similarly superimposed for bolted joints.

Knowing the load transfer rate (LO) and the individual tension intensities (k_{BY}, k_{LT}) for both notch loads and their dependencies on the corresponding influence parameters, dimensioning can be carried out for a laminate with regard to the failure in the remaining cross sections (side fracture).

The influence parameters of the load transfer rate are primarily located in the stiffness of the plate sections and in the stiffness of the joint elements and their number in the load direction. Semi empirical research on this topic can be found in Tate, Rosenfeld [8], and Huth[9], among others.

2.3 Testing Program

In order to determine the notch loading factors, approx. 900 tests were carried out in order to provide information on the dependency of different parameters.

Stiffness at a 100% bypass were determined based on corresponding open-hole tests.

Different bolted joint structures were tested as well. The main focus of this program therefore is on different, typical parameters of bolted joints. Insights on joints and the influence of different load transfers, bending influence and additional parameters (bolt material, abatement, secondary bending) are analyzed here.

The tests were carried out in constant geometrical conditions with regard to width, edge distance, and pitch. On the other hand, absolute parameters with regard to bolt diameter and thickness of the sample were changeable. Bolt diameters of 11.11 mm to 25.40 mm and sample thickness of 15 mm to 30 mm were examined.

These examinations were carried out with the HTS 6376 UD tape with a single layer thickness of 0.25 mm. Two different laminate structures were tested: a skin laminate (50/40/10) and a spar laminate (10/80/10). Tests and joint pieces were made of the same laminate structure. HI-LOK bolts were used for all tests whereby different bolt materials (titan and steel) and forms (countersunk and protruding heads) were tested. A clamping torque fitted to the bolt

diameter (according to manufacturing standards) was provided for all tests.

The load transfer rate of the bolted joints was determined with the aid of an optical elongation measurement. Stochastic patterns were applied to the surface of the samples and were taped with a video camera before and during the loading (see Fig. 4). Elongation in different directions can be determined when comparing the figures [10].

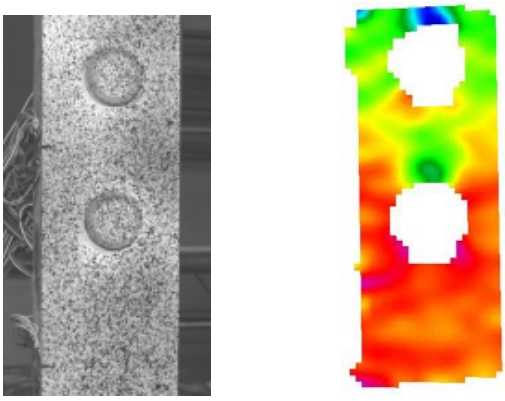

Fig. 4. Elongation measurement: „pre-treated sample“ (l.) and deformation result (r.)

2.4 Analysis of the Results with Regard to a Design Rule

The necessary parameters for the calculation of the superimposition function can be determined by the tests. These, however, are dependent on different parameters and in different forms. All of the mentioned influence parameters could not be examined so that some correlations were only able to be interpreted from certain geometric and manufacturing viewpoints. As already mentioned, the main focus is to study the influence of the laminate thickness on bolted joints.

Samples with unloaded holes were used for tension intensity at a 100% bypass. It becomes clear that, in addition to the laminate, the main parameter in such a study is primarily the diameter. A positive result of the tests is that the thickness of the samples did not have a reduced effect. In Fig. 5 the notch stress factor between 15mm and 30mm is applied as a function of the diameter in the thickness of the laminates.

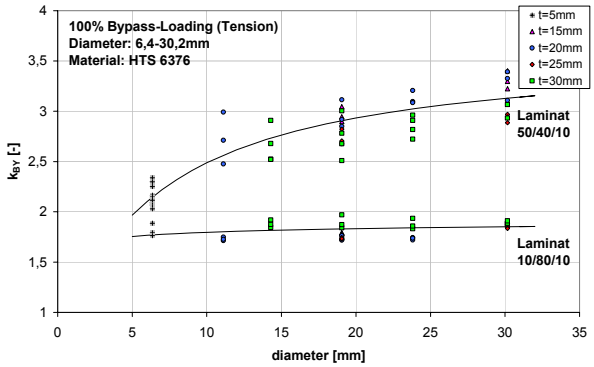

Fig. 5. Notch stress factor at a 100% bypass

This figure clearly shows the increase of the notch stress factor with the diameter of both laminates. It is noticeable that the stiffer skin laminate (50/40/10) apparently is more notch sensitive than the spar laminate (10/80/10).

In order to determine the notch loading factors during load transfer, 2 and 3-rowed joints with regard to a 100% loading transfer were converted with the help of Eq. 5.

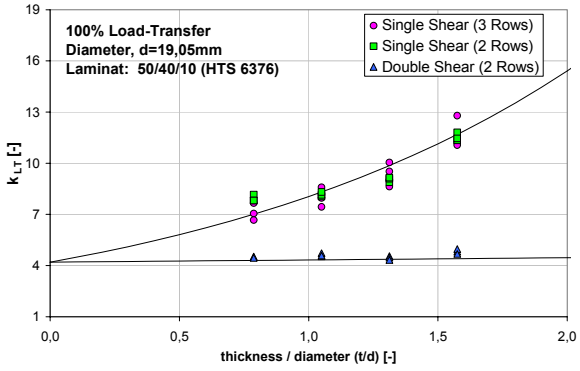

Fig. 6. Notch loading factor at a 100% load transfer (d=19.05mm, 50/40/10)

Because of the uneven distribution of tension over the height of the laminate caused by the bolt deformation, it becomes clear that the notch loading factor is heavily dependent on the thickness / diameter ratio (t/d) (see Fig. 6). Here the difference between single and double-shear configurations becomes clear. Single-shear samples are much more dependent on the t/d parameter due to strong bolt deformations. Extrapolating the single and double-shear values (t/d->0) they lead in a common notch stress factor. This is regarded as notch loading with neglect able bolt deformation (plane problem). The notch loading k_{LT}(t/d=0) may be a theoreti-

cal parameter but proves to be very useful in the formulation of the notch loading factors for the load transfer.

Together with the determined notch loading factors, the dimensioning guideline now provides the strengths of single and double-shear joints as a function of the load transfer. A dimensioning of the bolted joints can be made with the knowledge of the geometrical boundary conditions and the load transfer rate.

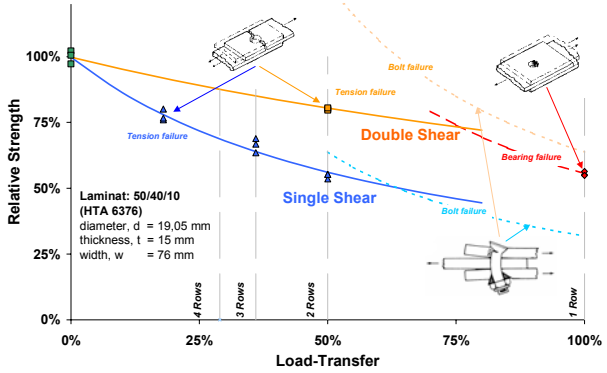

Fig. 7. Tension intensity factor at a 100% load transfer

In Fig. 7 an example of the correlation for single and double-shear joints is shown for a laminate and a geometry. The dots represent tests for the corresponding geometry for single and double-shear joint configurations.

A decrease in the strength as the rows decline and thus an increase of the load transfer as well as a difference in the strength between single and double-shear joints become evident.

A statistical evaluation of the deviation of the design rule from the strength results shows that the standard deviation is around 5% when both parameters are placed in direct proportion. This also lies approximately in the area of the scattering of the results and shows that the influence parameters have been registered well enough.

Statistical research for fatigue tests was supplemented with R=0.1. No failure of the laminate was observed in these tests, making it seem unnecessary to take the repeated loading during the design of the laminate into consideration.

3 Design Rules for Rib Stability

In this chapter, a design rule for the stability of unstiffened whole wall ribs with and without notches is described. Additional Design Rules are described in Herbeck et. al. [14]. In addition to an analytical and a FE calculation, an optimization of the ribs and an examination of the test calculations using DMS and a 3D grid process are presented. The ribs can be calculated here as a plate beam.

3.1 Calculation of the Rib Stability

3.1.1 Analytical Calculations

An estimation of the critical buckling loads can be made analytically. First the ribs are idealized as a flexibly supported rectangle. The actual support at the connections to the wing shell and the joints with the spars will be somewhere between “clamped” and “flexibly supported”. Choosing the flexible support is always better since the buckling loads here are lower than with those that occur with clamping.

Calculation of the stability of the unstiffened plate can be conservatively estimated by means of the “combined buckling hypothesis”. Compare:

$$\frac{n_z}{n_{zkr}} + \left(\frac{n_{yz}}{n_{yzkr}}\right)^2 \le 1 \qquad (6)$$

Critical buckling pressure and shear flow are assumed under the following conditions:

- if the main orthotropy axes (1, 2) run in the direction of the rectangle sides,
- if the laminate is symmetrical to the middle level and
- if the calculated buckling flows are within the linear-elastic area

for the shear flow by:

$$n_{yzkr} = k_s \left(\frac{\pi}{b}\right)^2 \sqrt[4]{D_{11} D_{22}^3} \qquad (7)$$

and for the critical pressure flow by

$$n_{zkr} = k_D \left(\frac{\pi}{b}\right)^2 D_{11} \qquad (8)$$

The buckling coefficients ks and kD are indicated in dependence of the effective side ratio

$$\alpha = \frac{b}{a}\sqrt[4]{\frac{D_{11}}{D_{22}}} \qquad (9)$$

which is also relevant to the bending stiffness of the plate, and the Seydel orthrotropy parameter

$$\eta = \frac{D_{12} + 2D_{33}}{\sqrt{D_{11}D_{22}}} \qquad (10)$$

in [11] in the form of curved shells. The ribs that are to be studied here have a geometrical height-to-width ratio of 0.2. Therefore they can all be calculated as plate beams. The pressure buckling value k_D for all flexibly supported, orthotropic plate beams amount to 1, see [13]. The shear buckling value, on the other hand, still depends on the Seydel orthrotropy parameter, the so-called cross number. It can be approximated with the following equation:

$$k_s = 3{,}3 + 2{,}5\,\eta - 0{,}18\,\eta^2 \qquad (11)$$

Since the precise stacking order of the laminate and the elements of the composite bending stiffness matrix are not yet known during the design phase, calculations can be made more easily with the middle bending stiffness

$$D_{11} = \frac{E_x t^3}{12\left(1 - \nu_{xy}\nu_{yx}\right)}, \qquad D_{22} = \frac{E_y t^3}{12\left(1 - \nu_{xy}\nu_{yx}\right)}, \qquad (12)$$

$$D_{12} = \nu_{xy}D_{22} = \nu_{yx}D_{11}, \qquad D_{33} = \frac{G_{xy}t^3}{12}$$

These result under the assumption that the plies of each fiber orientation are evenly distributed over the plate thickness so that a homogeneous plate is created. Depending on the actual order of the layers, the calculated, middle buckling flows (Eq. 8 and 9) can deviate from the actual buckling flow.

The analytical stability calculation of the notched ribs is not possible since the decline of the buckling value due to a notch is not known. In order to still obtain a quick estimation of the critical buckling load, comprehensive FEM calculations and tests were carried out, the results of which are presented in the chapter on stability.

3.1.2 FEM Calculation

The finite element calculations of the rib stability were made with the isoparametric four-knot shell element QUAD4 from the MSC/NASTRAN library that are based on bi-linear approach functions. The MSC/PATRAN program was used for modeling and networking, whereby the LAMINATE-MODELER was used to define the multi-layer laminate. Based on the classical laminate theory, fiber composite materials can be generated layer by layer from the previously defined UD single layers. In addition, the CADFEM/ANSYS program package was used for linear calculations.

First, linear stability calculations were carried out by means of eigenvalue analyses which supply explicit buckling loads and their respective buckling forms with arbitrarily normed amplitudes.

In order to make a correlation between the load levels of the experiments and the amplitudes of the buckling form, a non-linear calculation was then performed. A small imperfection in the form of a buckling shape determined by linear FEM was added onto the structure and then the load was added in several steps.

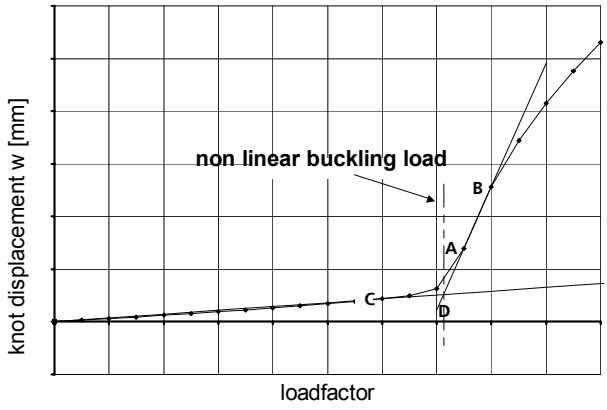

Fig. 8. Non linear FEM calculation of the samples: graphic determination of the stability limit.

In order to precisely determine the occurrence of the stability case, knot displacement w to the plate level of a selected knot is shown above the load. An evaluation diagram is shown in Fig. 8 as an example in which guide lines necessary for the evaluation are depicted. A tangent is applied to the curvature that runs through points A and B. The second guideline is given

by the extrapolation of the quasi-linear uncritical deformation area (C). From the intersection point (D) of the tangent and guideline a perpendicular line is run to the load axis and marks the non linear critical buckling load.

3.2 Optimization of Notched Ribs

During optimization of the unstiffened notched ribs, the only free parameter is the laminate set-up. If the ribs are primarily loaded with pressure, the most reasonable choice is a laminate set-up with a high 0° share of plies (in the force direction). As for the tested ribs that were primarily loaded with shear, the optimum stability is almost independent of the chosen laminate set-up, as can be seen in Fig. 9. This is because the high shear buckling value has small stiffness as a result and vice versa. This leads to almost similarly critical shear flows over the entire force area of interest and therefore the required wall thickness.

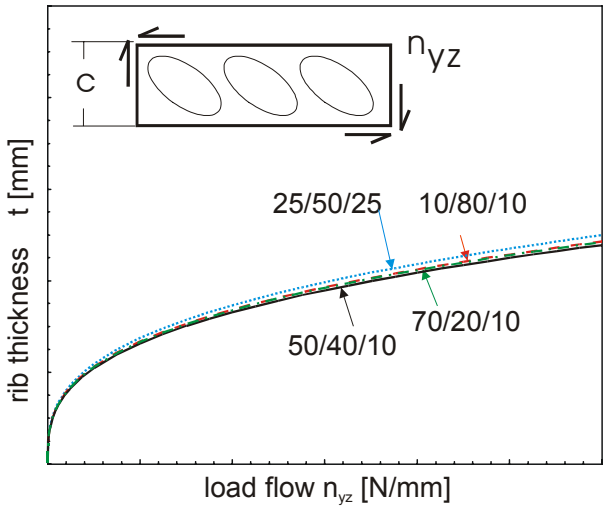

Fig. 9. Influence of the stacking sequence on the required critical buckling wall thickness

The optimization for the notched ribs depends on the requirements for optimal strength. For both of the prevalent rib types this would be the laminate set-ups [10% 0°/ 80% ±45°/ 10% 90°] primarily for shear loads and [50% 0°/ 40% ±45°/ 10% 90°] with even pressure and shear loads.

3.3 Stability Test Evaluations

3.3.1 DMS Evaluation

The evaluation of the tests that were carried out [15]to determine the empirical buckling load was made by means of a graphic determination with the aid of a special evaluation diagram. The opposing elongation measured value sequences of a measurement area are shown above the test force. As an example, Fig. 10 shows the measured value sequences resulting from non-linearity that occurred during buckling. A more common term for this is funnel curves. At the same time, a third curve in this diagram that represents the arithmetic mean value between elongation measured value sequences was also shown above the test force.

Tangents are shown in the linear overly critical area of the funnel curves. Starting a the points of intersection of the two tangents with the mean value curves lines run perpendicular to the load axis and show the empirical buckling limits of this measurement. The arithmetic mean value between the upper and lower empirical buckling limit is defined as an experimentally determined buckling load for the observed measurement area.

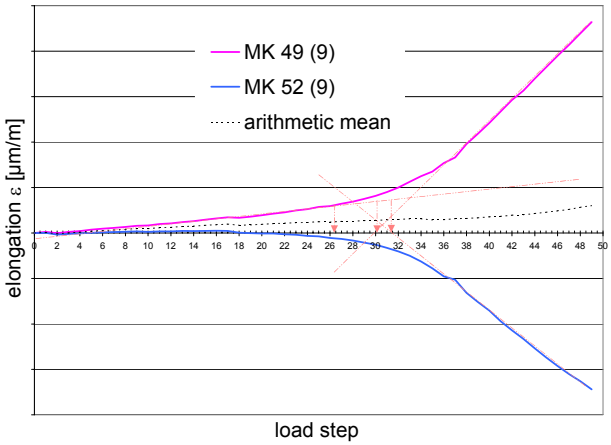

Fig. 10. DMS evaluation of a shear test of sample body

This graphic evaluation is carried out at each measurement area within the test for all measurement directions (0°, 45°, 90°). Within the values of each measurement direction, the smallest value is defined as the buckling differ-

ence for that measurement direction and is then arithmetically averaged.

3.3.2 Evaluation of a 3D Raster Method

In addition to the DMS measurements, 3D grid measurements were carried out on all samples (see [16]). The 3D grid method is an optical measurement method that enables the determination of displacement fields, among other things.

The order of the images in Fig. 11. indicates the changes that take place in the buckling shape depending on the type of load. The buckling in Fig. 11a is below 45°. With an increase in the share of pressure it is oriented to a 0° pressure load direction as seen in Fig. 11d.

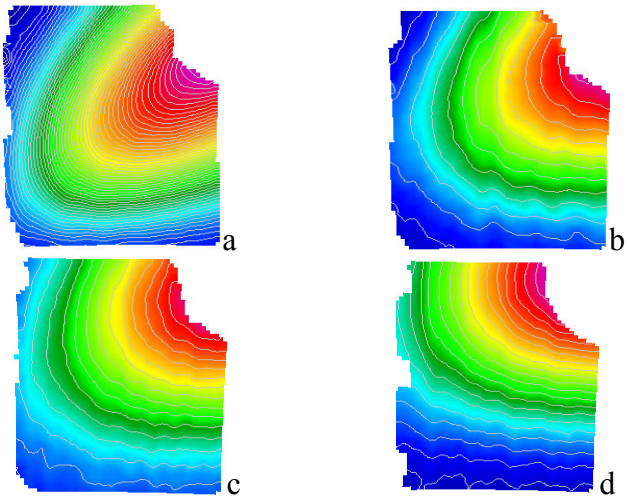

Fig. 11. Changes in the buckling shape with changed load forms a) shear loading n_{xyz}, b) $n_{yz}/n_x = 5$, c) $n_{yz}/n_z = 1$, d) pressure loading n_z

3.4 Design Rules Stability with Notches

The below figure (Fig. 12) shows an interaction diagram for a combined notched pressure-shear loading. The FEM calculation results for flexible support and clamping are recorded here. The results of the individual buckling tests are noted as well. The diamond stands for the chosen buckling value, the cross for the lowest buckling level and the circle stands for the highest buckling level. All test results tend to lie between the FEM results of the flexible support and the results of the tight clamping. The result of this comparison is that the flexible support demonstrates a conservative estimation of the critical buckling values of the notched ribs under a combined pressure-shear loading.

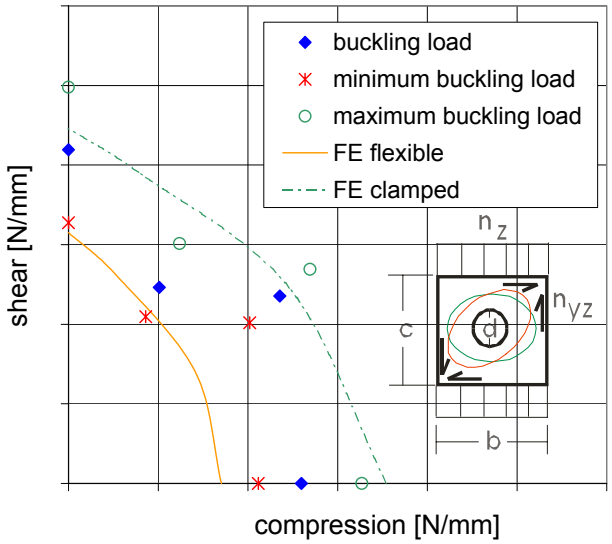

Fig 12. Interaction diagram of the buckling of notched ribs

If the FEM calculation results of a flexible support of an unnotched rib are normed, the result is a stability declination factor based on the relative notch size, see Fig. 13. This, in turn, depends on the chosen stacking sequence. The declination factor does not continue to decrease with greater notches but increases again with a high share of shear stacking. These surprising results correspond well with the test results.

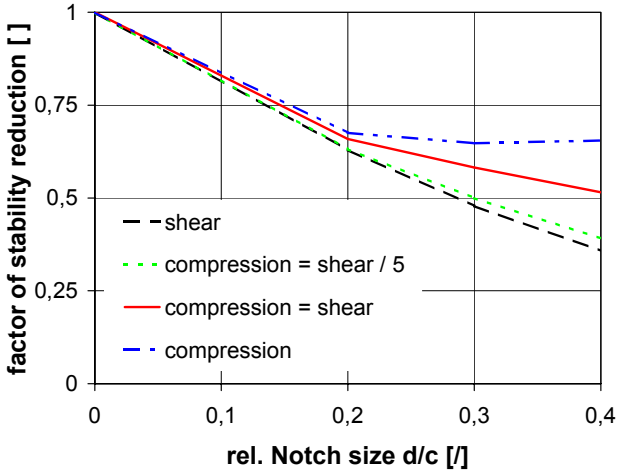

Fig. 13. Design Rule: Declination factor of the stability for notched ribs, laminate 50/40/10

Nomenclature

α	effective side ratio
η	Seydel orthotropy parameter
ε_x	elongation in the x direction
γ_{xy}	shear strain in the x, y directions
ε_y	elongation in the y direction
σ	*tension*
B_{X1}, x_2	bending stiffness on the pressure and
c	height of rib
d	notch diameter
D_{ij}	plate bending stiffness of rib
$E_{x,y}$	elasticity module in x and y directions
F	*force*
G_{xy}	shear module in the x, y levels
k	*notch loading factor*
k_s, k_D	buckling coefficient
l	width of ribs
$L0$	*loading share due to load transfer*
n_z, n_{yz}	pressure force flow
n_{zkr}, n_{yzkr}	critical buckling pressure flow, shear flow
t	*thickness*
	tension sides
v	ratio of support requirement
w	*width / displacement*

Signs

BY	*Bypass Loading*
LT	*Load Transfer*
max.	*maximum*
r	*radial*
t	*tangential*

Acknowledgements

The authors appreciate the support of the whole common Airbus Germany / DLR Design Rule team. Many thanks to: Mr. Becker, Dr. Mühlmann, Dr. Schrader, Mr. Kröber, Mr. Schieber and Mr. Bitter.

References

[1] Sawin G.N. *Spannungsüberhöhung am Rande von Löchern*. VEB Verlag Technik, Berlin 1956

[2] Awerbuch J, Madhurkar M S. Notched strength of composite laminates: Predictions and experiments – A Review. *Journal of Reinforced Plastics and Composites*, 1985

[3] Hart-Smith L J. Mechanically–fastened joints for advanced composites-Phenomenological considerations and simple analyses. *Fibrous Composites in structural Design*, Plenum Press, New York 1980

[4] Herrington P D, Sabbaghian M. Effect of radial clearance between bolt and washer on the bearing Material of composite bolted joints. *Journal of composite materials*, Vol 26, 1992

[5] Collings T A. Experimentally determined strength of mechanically fastened joints. *Joining Fibre-Reinforced Plastics*, Matthews I. Elsevier Applied science, 1987

[6] Whitney J M, Nuismer R J. Stress Fracture Criteria for laminated Composites Containing Stress Concentrations. *American Society of Testing and Materials*, 1975

[7] Jarfall L. *Shear loaded fastener installations*. Rapport KH R-3360, Saab Scandia, Sweden, April 1993

[8] Tate M B, Rosenfeld S J. Preliminary investigation of Loads carried by individual bolts in bolted joints. *TN No. 1051, Langley Memorial Aeronautical Lab.*, Washington, May 1946

[9] Huth H. *Zum Einfluss der Nietnachgiebigkeit mehrreihiger Nietverbindungen auf die Lastübertragungs- und Lebensdauervorhersagen*. Fraunhofer Institut für Betriebsfestigkeit, Dissertation TU München, August 1984

[10] Wilmes H, Behring D. *Ermittlung der Einflussgrößen der Lastübertragung bei CFK-Bolzenverbindungen anhand von optischen Dehnungsmessungen*. IB 131-2000 / 09, Braunschweig, 2000

[11] Herbeck, L, Schrader E, Becker H W, Mühlmann H-C, Bitter H. Die Stabilität der Rippen eines CFK_Außenflügels am Beispiel des Airbus-Megaliner. *Deutscher Luft- und Raumfahrtkongress/ DGLR-Jahrestagung,* Leipzig, 18.-21.09.2000, Deutsche Gesellschaft für Luft- und Raumfahrt (DGLR), Leipzig (2000).

[12] Luftfahrttechnisches Handbuch (LTH), *Handbuch Strukturberechnung (HSB).* herausgegeben vom Industrieausschuß Strukturberechnung (IASB)

[13] Wiedemann J. *Leichtbauelement. 2*. Aufl. Springer-Verlag Berlin Heidelberg New York 1996.

[14] Herbeck L, Schrader E. *Design Rules für den Megaliner 2010 CFK-Außenflügel: Stabilität unter kombinierter Schub/ Druckbelastung: Versuchsreihe RA.* DLR Institut für Strukturmechanik – Interner Bericht IB 131 - 99 / 52, Braunschweig1999.

[15] Oesmann H W. *CFK – Flügel / Megaliner – Delta – Programm, Rippen / RA; Statische Untersuchungen zur Stabilität an Rippenabschnitten bei kombinierter Druck- / Schubbelastung*. DaimlerChrysler Aerospace Airbus GmbH Technical Note: TN-EVS - 3840 / 99, Hamburg 1999.

[16] Galanulis K., Winter D. *Optische Verformungsmessung zur Bauteildimensionierung am Beispiel von KFZ-Getrieben*. Technisches Messen 62 (1995) 1, Oldenbourg Verlag, s. 3-8.